A Combined Finite Element-Multiple Criteria Optimization Approach for Materials Selection of Gas Turbine Components

A. Shanian[1]
School of Engineering and Applied Sciences,
Harvard University,
Cambridge, MA 02138,

A. S. Milani
School of Engineering,
University of British Columbia-Okanagan,
Kelowna, BC, V1V 1V7, Canada

N. Vermaak
Materials Department,
University of California Santa Barbara,
Santa Barbara, CA 93106

K. Bertoldi
School of Engineering and Applied Sciences,
Harvard University,
Cambridge, MA 02138

T. Scarinci
Rolls-Royce Canada,
9500 Cote de Liesse,
Dorval, QC, H8T 1A2 Canada

M. Gerendas
Rolls-Royce Deutschland Ltd. & Co KG,
Dahlewitz, 15827, Germany

The design of critical components for aerospace applications involves a number of conflicting functional requirements: reducing fuel consumption, cost, and weight, while enhancing performance, operability and robustness. As several materials systems and concepts remain competitive, a new approach that couples finite element analysis (FEA) and established multicriteria optimization protocols is developed in this paper. To demonstrate the approach, a prototypical materials selection problem for gas turbine combustor liners is chosen. A set of high temperature materials systems consisting of superalloys and thermal barrier coatings is considered as candidates. A thermomechanical FEA model of the combustor liner is used to numerically predict the response of each material system candidate. The performance of each case is then characterized by considering the material cost, manufacturability, oxidation resistance, damping behavior, thermomechanical properties, and the FEA postprocessed parameters relating to fatigue and creep. Using the obtained performance values as design criteria, an ELECTRE multiple attribute decision-making (MADM) model is employed to rank and classify the alternatives. The optimization model is enhanced by incorporating the relative importance (weighting factors) of the selection criteria, which is determined by multiple designers via a group decision-making process. [DOI: 10.1115/1.4006461]

Keywords: multiple attribute decision-making, gas turbines, design, material selection, FEA

1 Introduction

The high reliability required in the design of sensitive components, such as gas turbines, has made their materials selection a critical task (Shanian et al. [1]). Considerable attention has been paid to select appropriate materials from existing databases that provide a relatively low cost manufacturing process and high thermomechanical performance [2]. In particular, the high strength-to-weight and stiffness-to-weight properties of advanced superalloys, ceramic-based composites, and hybrid materials have gained the attention of several manufacturers for structural applications in combustion systems [3,4]. To take full advantage of high temperature materials, however, their selection should be made with expert knowledge. This is often a challenging task due to the variety of possible solutions and trade-offs between properties of candidate materials. As a first step, the designers' experience and analysis tools should be used to identify/short-list candidate materials. Recently, Aceves et al. [5] presented a methodology to identify a short list of structural materials from a large number of alternatives, taking into account conflicting design objectives and constraints. After a short-listing procedure, designers are often left with a few candidate materials that show no apparent dominance over one another. A material may be outperforming others under a particular set of criteria but is inferior under some other criteria. This situation can be more pronounced when a large number of design criteria need to be simultaneously satisfied (e.g., thermal, mechanical, cost, etc.). Ashby recommended materials selection charts for a wide range of engineering applications [6–9]. The materials selection procedure in this method is performed based on two or three performance indices per chart. Applications of the method for lightweight materials are seen in a number of earlier works. Valdevit et al. [10] developed a materials selection protocol for lightweight actively-cooled panels where failure maps were used to allow direct comparison of materials' thermal and mechanical performances. Another study by Sadagopan and Pitchumani [11] used genetic algorithms for material selection of structural components in conjunction with analytic microstructure-property relations.

Thurston and Carnahan [12] presented an application of fuzzy set analysis and multiattribute utility theory for materials selection in the preliminary design stage of some automotive applications. Karandikar and Mistree [13] developed a multiobjective optimization-based technique for assisting designers in tailoring composite/hybrid materials for specific technical and economic objectives. Fitch and Cooper [14] presented life cycle energy analysis as a method for materials selection. A set of life cycle energy variables was created to distinguish between energy consumption that occurs during different phases of a product's life cycle. More recently, local Taylor-series approximations and strategic experimentation techniques have been developed by Seepersad et al. [15] for assessing the impact of dimensional and topological imperfections, respectively, on material properties and the interactive selection of materials.

Fayazbakhsh and Abedian [16] discussed the application of a Z-transformation method in materials selection. Among other related published work, when simultaneously evaluating and comparing the performance of materials under a large set of design criteria, mathematical solutions of large decision spaces have been based on the so called 'multiple attribute decision making (MADM)' methods [17]. In MADM, the decision variables

[1]Corresponding author.

Contributed by the Applied Mechanics Division of ASME for publication in the JOURNAL OF APPLIED MECHANICS. Manuscript received July 6, 2011; final manuscript received March 19, 2012; accepted manuscript posted March 29, 2012; published online September 26, 2012. Editor: Marc Geers.

(attribute values) can be quantitative or qualitative, Boolean or continuous, deterministic or probabilistic. The possibility to include uncertainties associated with material data using MADM has also been the subject of earlier investigations; see, e.g., Ref. [18].

The contribution of the published methods for screening and determining optimal materials and processes has been summarized in a comprehensive review by Jahan et al. [19]. It was concluded that the application of multicriteria decision-making approaches can greatly improve the materials selection procedures and allow decision makers much greater flexibility in terms of selection criteria, preferences, and uncertainties. There are several types of MADM models such as compensatory versus noncompensatory, quantitative versus qualitative, scoring versus ranking, classifications that can be used by designers to treat various materials selection scenarios. In contrast to some of the earlier materials selection methods, in MADM, all selection criteria can be simultaneously evaluated.

Most materials selection methods reviewed in the preceding text employ material databases from handbooks (e.g., to extract material properties) and/or performance indices that are based on analytical formulas for simplified structural components (such as plates, shells, bars, laminates, etc.). In addition, it may not be economically feasible to provide manufacturing and testing data for different materials at the early stages of a design. As a result, in these stages, the material and structural assessments can rely on numerical prediction tools such as finite element analysis (FEA). There is little or no effort to link the higher order capabilities of the FEA in predicting the performance of complex design candidates with the mathematical capabilities of decision-making models to optimize the materials selection of structures in the early stages of a design.

To address this gap, especially in the field of gas turbine design, this article presents a combined FEA-MADM multiple criteria materials selection protocol that demonstrates the possibility to systematically evaluate the material and structural trade-offs before the actual manufacturing takes place. Multiple criteria materials selection for a gas turbine liner by a group of designers is used as a case study. The performance measures selected include: the material cost, oxidation resistance, thermomechanical properties, damping behavior, fatigue, and creep parameters.

2 Case Study: Materials Selection of a Combustor Liner

The ability to increase the firing temperature and improve emissions control motivates the materials selection for combustor liners. Materials that provide higher thermomechanical properties with oxidation/corrosion resistance are required. In combustors, wall temperatures are extreme and abrupt temperature changes are experienced during start-up and shutdown cycles. Thermal stresses can be significant due to large gradients from wall cooling processes. Additionally, due to the cyclic loading, high cycle thermal fatigue is a potential failure mechanism. Materials commonly used in today's combustor liners include C263, Re41, Waspaloy, and Haynes 282 [20,21].

The materials R-41 and Waspaloy have high yield and creep strengths at high temperature. However, they also have poor fabricability, especially in terms of weldability. The materials C263 and H-282 feature good fabricability while maintaining strength at high temperatures [20]. Current techniques for moderating the metal liner temperatures involve the use of thermal barrier coatings (TBCs) and the application of cooling air/holes.

Combustor components made of nickel-based alloys have generally performed well in most types of gas turbines, but as higher firing temperatures are desired, and more optimization-driven combustor design methodologies become available, there is a need to re-evaluate superalloy candidates such as C263, Re41, Waspaloy, and Haynes 282. This case study presents a combined

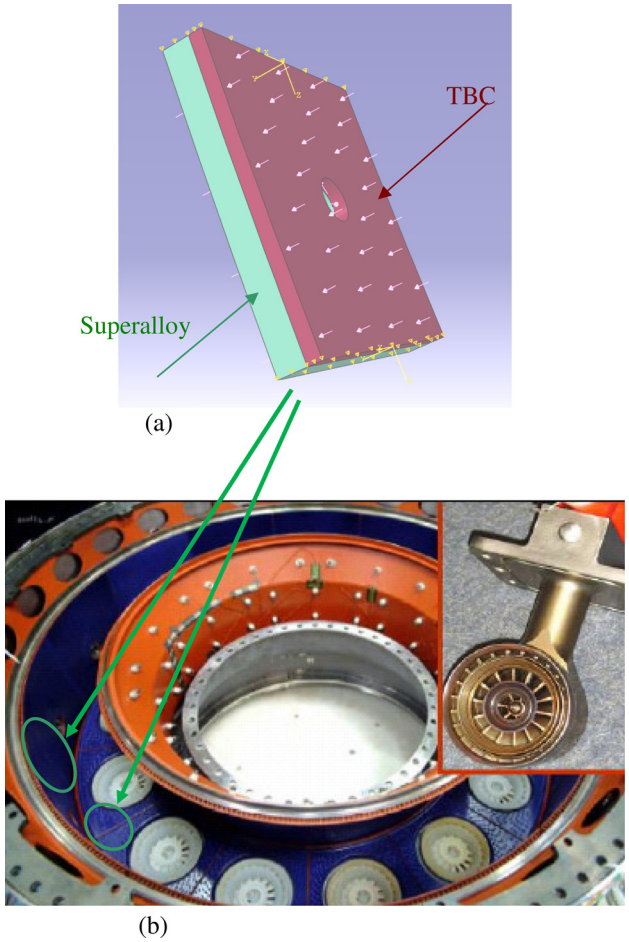

Fig. 1 (*a*) Unit-cell model using a 1/180th sector (the unit-cell view has been scaled for better visualization); the top surface of the wall is coated with a 300 micron 7 wt. % YSZ thermal barrier coating. (*b*) A prototypical annular combustor [21].

FEA-MADM approach for the previously discussed evaluation that is normally required in the early stages of a combustor design process. It is assumed that the design space of interest is identified by using manufacturing constraints and analytic estimates of key parameters before the FEA-MADM approach is applied. In this way, a grid of the relevant design space can be determined using a finite number of FEA simulations. More specifically, in the following example, the geometry is fixed while the material is varied. In more complex cases, both the geometry and material parameters may be varied together, although adding to the computational cost.

2.1 Finite Element Model

2.1.1 Fully Coupled Thermomechanical Analysis. A prototypical annular combustor wall unit cell (Fig. 1) was modeled in the ABAQUS FEA package. Annular combustors, as opposed to 'can combustors,' have a continuous liner and casing in a ring (the annulus), providing a number of advantages including more uniform combustion (with uniform exit temperature), shorter size (decreasing weight), less surface area, and very low pressure drop (on the order of 5%).

The unit cell representing the combustor wall in Fig. 1 consists of a superalloy layer that is protected by a zirconia-based thermal barrier coating (TBC, 300 micron 7 wt. % YSZ). The wall also includes a through-hole cooling channel which is bound by lines of symmetry in the system. The 1/180th sector annular wall is subject to three simultaneous loads: external pressure from the

Table 1 Combustor liner material properties used in the FEA simulations [20,24]

Temperature (K)	Thermal expansion (micron/m/K)	Yield stress (MPa)	Thermal conductivity (W/mK)
Haynes 282			
295.00	12.1	699	10.3
873.15	13.5	631	20.5
973.15	13.7	625	24.8
1073.15	14.2	580	26.1
1173.15	14.9	396	27.3
1273.15	16.9	75	28.9
C263			
295.00	11.1	585	11.72
873.15	13.9	490	21.35
973.15	14.6	495	23.03
1073.15	15.3	460	24.70
1173.15	16.5	145	26.80
1273.15	17.4	70	28.74
Waspaloy			
295.00	13.9	910	12.6
873.15	14.3	620	15.7
973.15	14.8	770	19.1
1073.15	15.4	770	20.9
1173.15	16.4	415	22.7
1273.15	17.8	135	24.5
Rene 41			
295.00	13.5	1000	11.5
873.15	14.0	950	21.0
973.15	14.8	930	22.0
1073.15	15.2	890	24.1
1173.15	15.7	850	25.1
1273.15	16.8	556	26.0

Table 2 Temperature-dependent properties of the thermal barrier coating (TBC) used in the simulation

Temperature (K)	Thermal expansion (micron/m/K)	Yield stress (MPa)	Thermal conductivity (W/mK)
949	11	40	2
1171	11	34	2
1282	11	26	2

combustion gases, internal pressure from the cooling air, and thermal loads due to the temperature gradient between the combustion side and the back of the combustor wall. Symmetry boundary conditions were applied on opposing faces in the circumferential and axial directions. The remaining surfaces are traction free. The total combustor wall thickness is 1.5 mm, the combustor radius is 298 mm, and the cooling hole diameter is 1.6 mm.

The temperature-dependent material properties used in the FEA simulations are reported in Tables 1 and 2. The superalloy candidates (Haynes 282, C263, Waspaloy, and Rene 41) are modeled as elastic perfectly plastic. Each design alternative consists of one of the previously discussed superalloy materials and a TBC layer. The FE mesh of the combustor wall uses 8-node trilinear coupled temperature-displacement elements (C3D8RT). Convective boundary conditions and pressure loads were applied to the top face, subject to the combusting gases ($h_g = 0.46$ mW/mm^2 K, $T_g = 1532$ K, $P_g = 1.95$ Mpa), the internal cooling hole surface ($h_{ch} = 1.993$ mW/mm^2 K, $T_{ch} = 580$ K, $P_{ch} = 1.98$ Mpa), and the back face surface within the vehicle interior ($h_b = 0.792$ mW/mm^2 K and $T_b = 480$ K, $P_b = 2.02$ Mpa) [22]. The remainder of the cell perimeter is thermally insulated. Numerical results for the four

Table 3 Output of FEA simulations for the four superalloy candidates

Design candidates	Maximum Von-Mises stress in the unit cell (MPa)	Maximum superalloy temperature in the unit cell (K)
1: H282	640	889
2: Re-41	957	888
3: Waspaloy	662	893
4: C263	586	888

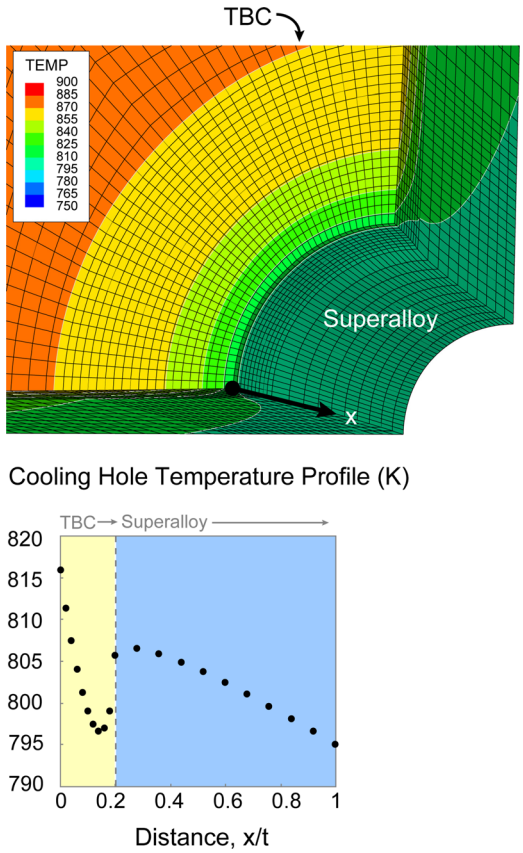

Fig. 2 FEA results for the H282 case; the contour shows the nodal temperature (K) for one-quarter of the unit cell. A line profile of the temperature is plotted as a function of the nondimensional distance through the thickness *t* of the combustor wall (including both the TBC and superalloy).

candidate designs (i.e., using four different superalloys) are summarized in Table 3. Sample temperature and stress contours for the H282 case are presented in Figs. 2 and 3.

2.1.2 Damping Behavior of the Candidates Via FE Eigenfrequency Analysis. Burner and furnace systems, including combustors, are generally sensitive to thermoacoustic vibrations due to the presence of a large temperature gradient between the cold air and the hot gases. As a result, the damping characteristics of such systems can play an important role in controlling excessive vibration amplitudes and eventual failure.

The modal strain energy (MSE) method was used to predict the damping performance of each design scenario (candidate) in the current study. The method has been proven to be an accurate predictor of damping levels in structures comprising layers of elastic and viscoelastic elements [23]. Using the MSE method, the damping coefficient for a given structural mode of vibration is found as the sum of products of the effective fraction of modal strain

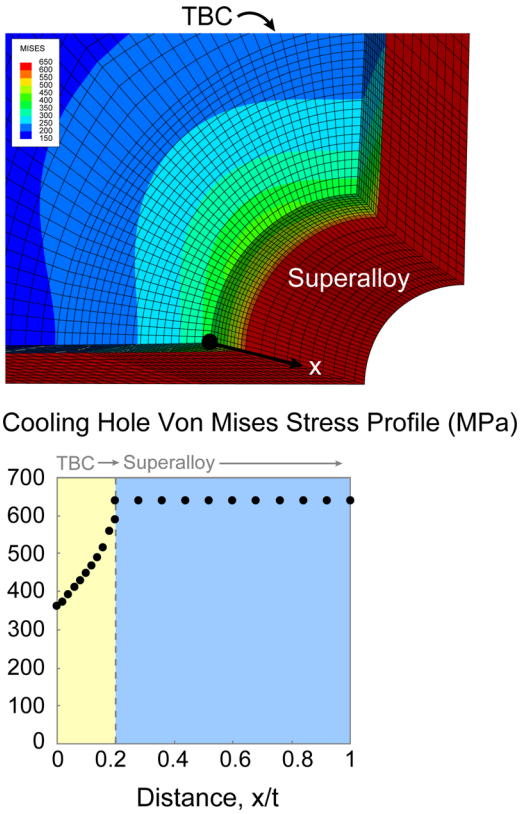

Fig. 3 FEA results for the H282 case; the contour shows the stress distribution in MPa for one-quarter of the unit cell. A line profile of the Von Mises stress is plotted as a function of the nondimensional distance through the thickness *t* of the combustor wall (including both the TBC and superalloy).

energy created in each layer of the material system by the effective loss factor of the corresponding layer [23]

$$\eta = \left(\frac{U_{superalloy}}{U_{total}} \times \eta_{superalloy}\right) + \left(\frac{U_{TBC}}{U_{total}} \times \eta_{TBC}\right) \quad (1)$$

η is the loss factor of the combustor cell, $\eta_{superalloy}$ and η_{TBC} are the loss factors of the superalloy and the TBC, $U_{superalloy}$ and U_{TBC} are the strain energy of each superalloy and ceramic layer, and U_{total} is the total strain energy in the cell.

Based on Eq. (1), it can also be inferred that the ratio of the material system's loss factor to that of the viscoelastic (TBC) layer for a given mode of vibration is proportional to the ratio of elastic strain energy in the viscoelastic layer to the total strain energy. The steps of the solution sequence for using Eq. (1) in the current case study were as follows:

- defining the material properties (elastic modulus, Poisson's ratio (ν), density, and loss factor) of each individual layer at maximum temperature
- computing the fundamental natural frequency of the cellular cell through FEM simulation
- comparing the total (cell) strain energy and the strain energy of each layer through FEM results
- computing the effective loss factor of the cellular cell based on Eq. (1)

The ensuing effective loss factors for different design candidates are included in Table 4.

3 Defining the MADM Problem

The decision criteria considered for the combustor liner materials selection in this case study are described in the following text and summarized in Table 5. In this table, under each criterion code, the positive and negative signs indicate the benefit- or cost-type attribute (i.e., the higher the better, the lower the better characteristics).

3.1 Oxidation Resistance. Resistance to oxidation at elevated temperatures is an essential requirement for the combustor liner material. The oxidation resistance performance index is defined by the amount of metal loss in the standard static oxidation test at a high temperature [20,21].

3.2 Cost. Material and manufacturing cost criteria are an important part of the selection process. In this study, the cost has been parsed into three main indicators: (1) cost of the base material, referred to as the cost performance index (a lower value is desirable); (2) the superalloy yield stress at room temperature (annealed condition) can indicate formability, a property usually associated with manufacturing cost. Typically good formability (low cost) is found in materials with low yield strengths; (3) high ductility is also desired since it is associated with lower manufacturing costs. Ductility is important because combustor liner materials must resist strain-age cracking due to post welding processes. This is often a limiting factor in utilizing high temperature alloys for combustor applications (see Pike [20,24]). With low ductility, combustor materials may not be able to accommodate residual stresses during post weld heat treatment (due to shrinkage during the solidification of the weld metal and the formation of a γ-prime phase). One way of quantifying the resistance to strain-age cracking is the controlled heating rate tension test, which evaluates the percent elongation, which is a measure of ductility, at high temperature. The higher ductility requirement for the post-weld process is the third index indicating manufacturing cost.

3.3 Thermal Fatigue. In service, gas turbine combustor liners are subject to cyclic loads which can result in high stresses and may induce failure through thermal fatigue mechanisms (thermal expansion/contraction effects [21]). The low cycle fatigue limit and the thermal expansion coefficient are often used to measure the thermal fatigue resistance of a combustor wall material. The number of cycles to initiate a crack (N_i), cycles to failure (N_f), and the thermal expansion coefficient of the combustor's superalloy material at the maximum working temperature (obtained by the FEA, Table 2), are used as the thermal fatigue performance indices.

Table 4 Effective loss factor prediction for each design candidate using the modal strain energy method at the maximum temperature obtained in Table 3; see also Shanian [25] and Limarga et al. [26]

Strain energy ratios from FEA			Individual loss factors $[(1/Q) \times 10^{-3}]$		
Design candidates	$U_{superalloy}/U_{total}$	U_{TBC}/U_{total}	$\eta_{superalloy}$	η_{TBC}	Effective loss factor $[(1/Q) \times 10^{-3}]$, Eq. (1)
1: H282	0.759984517	2.40×10^{-1}	4.0	0.5	1.26
2: Re-41	0.872573192	1.27×10^{-1}	4.0	0.5	1.37
3: Waspaloy	0.77573717	2.24×10^{-1}	4.0	0.5	1.28
4: C263	0.692928118	3.07×10^{-1}	4.0	0.5	1.19

Table 5 List of the decision criteria/performance indices used in the case study

Criteria category	Criterion code	Description
Creep	Cr1+	Larson-Miller parameter ($K \times 10^{-3}$, C = 20), comparative 1% creep data at 1500 to 1700 °F (816 to 927 °C)—age hardened sheet at maximum Von Mises stress; maximum Von Mises stress is obtained by FE simulation
	Cr2+	Stress-to-produce rupture in 1000 h at maximum operating temperature; temperature obtained by FE simulation
Oxidation resistance	O3−	Avg. metal affected (micron) obtained by static oxidation test data at (~1200 K)/1008 h. Handbook values.
Material cost and manufacturability	M4−	Yield at room temperature—mill annealed sheet (MPa) (higher value reduces the ease of formability). Handbook values.
	C5−	Cost of the base material. Handbook values.
	M6+	Controlled heating rate tensile tests: ductility (% at 816 °C) (higher value is good for preventing strain-age cracking during postweld processes). Handbook values.
Fatigue	F7+	1% total strain range at maximum superalloy operating temperature (temperature obtained by FE simulation). Number of cycles to initiate a crack (N_i in cycles).
	F8+	1% total strain range at maximum superalloy operating temperature (temperature obtained by FE simulation). Number of cycles to crack failure (N_f in cycles).
	F9+	Mean coefficient of thermal expansion (micron/m/K) at maximum superalloy temperature (temperature obtained by FE simulation).
Damping	D10+	Loss factor ($1/Q \times 10^{-3}$) of cellular cell at maximum operating temperature (temperature obtained by FE simulation).

Table 6 The case study MADM decision matrix (based on the units given in Table 5)

Aternative designs	Criteria code									
	F7+	F8+	F9+	Cr1+	Cr2+	M6+	M4−	C5−	O3−	D10+
H 282	908	1123	15.9	26	90	14.2	402	1	46	1.26
Re-41	924	1100	16	24	90	3.1	592	1.8	74	1.19
Waspaloy	840	1049	16.4	25	48	4.1	490	1.7	132	1.28
C 263	608	684	16.6	24.5	48	26	327	0.7	109	1.37

Table 7 Four designers' preferences based on the revised Simos' card play procedure ($z = 3$)

Designer no.	Importance levels		
	I	II	III
1	Cr1,Cr2,O3,M4,C5,M6,F7,F8,F9,D10		
2	O3,F7,F8,F9,D10	Cr1,Cr2	M4,C5, M6
3	Cr1,Cr2,O3,F7,F8,F9,D10	C4,C5,C6	
4	M4,C5,M6	Cr1,Cr2,O3, F7,F8,F9,D10	

3.4 Creep. The creep-related criteria chosen for this study are: (1) the stress required to produce rupture at maximum Von Mises stress (Table 2), and (2) the Larson-Miller parameter. A higher and lower value, respectively, is desired.

3.5 Damping. As discussed in Sec. 2.1.2, the damping behavior of each candidate material system can be evaluated through the total (cell) loss factor, which is essentially a measure of the effect of the loss modulus of the viscoelastic portion (TBC) of the material system. A higher cell loss factor is preferred since this could result in lower vibration amplitudes under thermoacoustic loads such as combustion shocks, etc.

The numerical values of the resulting decision matrix based on the preceding criteria are shown in Table 6 [25,26]. It is evident that no single material is ideal, given the conflicting tradeoffs in the selection criteria. For example, from Table 6 one can note that R-41 has a superior performance under the F1 fatigue criteria, but it has a poor value under the M4 manufacturability criterion. Conversely, H282 features good fabricability under M4 while exhibiting low performance under F1 (compared to R-41). The next task is to use a MADM solution method and rank the candidate materials based on the values of the decision matrix in Table 6. It is also of interest to implement a group decision-making process in which multiple designers can input their preferences (importance factors) over the criteria categories. These capabilities are addressed in the following section.

4 Solution: ELECTRE III With Group Decision Making

Four design experts were asked to complete the task of criteria weighting (i.e., outlining their preferences) for the combustor liner materials selection. Optimal solutions must take the material cost, manufacturability, oxidation resistance, damping behavior, thermomechanical properties, and fatigue and creep parameters into consideration (Table 5). The designers' preferences were as follows (see also Table 7):

- Designer No. 1: All criteria are of equal importance.
- Designer No. 2: Fatigue, damping, and oxidation resistance are of primary importance, followed by creep performance, and then cost and manufacturability.
- Designer No. 3: Fatigue, oxidation, damping, and creep performance are primary concerns. Cost and manufacturability are of secondary concern.
- Designer No. 4: Cost and manufacturability are the most important factors. Creep, oxidation, damping, and fatigue performance are all secondary.

The revised Simos' procedure was used to aggregate these preferences and derive overall weighting factors. Simos' method was originally developed by Figueira and Roy [27] for single decision-making processes and later was extended to group decision-making by Shanian et al. [1]. It is based on a 'card playing' procedure in which different criteria are classified into different levels (also called subsets) by each decision maker (DM), followed by the ranking and then weighting of subset levels. In the card play stage, the least important criteria fall on the left side (Fig. 4). Blank cards can be added to further distinguish between criteria. A ratio of the most important design criterion to the least important criterion z is also determined by the DM and added to the weight extraction procedure for normalization. The solution steps of this method have been summarized in the Appendix. The ensuing normalized weights are given in Table 8.

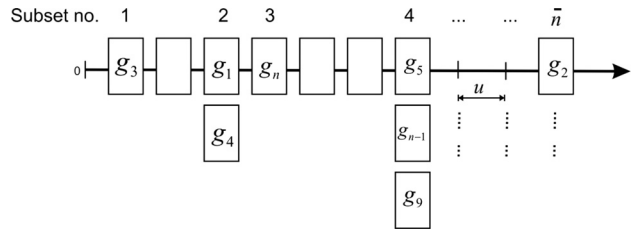

Fig. 4 Schematic of the card play by decision makers in the revised Simos' procedure (*u* is the distance between two adjacent subsets and is defined from the *z*-ratio)

Combining the weighting factors (Table 8) with the decision data (Table 6), the next task is to find the final ranking of the candidate materials. To do this, it is assumed that the values of the material properties or performance indices cannot directly compensate for each other. That is, a very poor performance of a material with respect to one criterion may not be excused by its favorable values under some other criteria. For this reason, only noncompensatory MADM approaches were considered.

Of the various ELECTRE noncompensatory methods that are well adapted to the revised Simos' weighting procedure, ELECTRE III was chosen. The method has been found to be reasonably robust when including data uncertainties in materials selection problems [1]. The ELECTRE III solution procedure starts by considering all n criteria (here $n=10$) in the decision problem as pseudocriteria (instead of true criteria) in order to include possible uncertainties in their measured values. To this end, for each criterion g_j $(j=1,...,n)$, an indifference threshold q_j, a strict preference threshold p_j, and a veto threshold v_j are defined (it is assumed that these thresholds are independent of the alternative performances). The indifference threshold can be chosen to represent the lower bound of uncertainty, while the strict preference threshold may represent the upper bound of uncertainty. The veto threshold represents a limiting value for the difference between the performance values of two arbitrary alternatives. The threshold values are considered up to 5–10% of the minimum difference, depending on the set of values for each criterion.

For each pair of arbitrary alternatives (i.e., design candidates) such as M_i and M_k $(i \neq k)$, an outranking relation (denoted by $M_i S M_k$ or $M_i \rightarrow M_k$) is examined. The relation implies that M_i outranks M_k if: (1) M_i is at least as good as M_k under the majority of criteria, and (2) M_i is not significantly bad under any other criteria. The trueness of the outranking relation is measured by calculating a credibility degree δ_{ik}. The credibility degree, in turn, is based on the definition of two fuzzy indices: the concordance index $c_j(M_i,M_k)$, and the discordance index $d_j(M_i,M_k)$. With respect to each criterion g_j $(j=1,...,n)$, the concordance index can take a value between 0 and 1 as

$$c_j(M_i,M_k)=\begin{cases}0; & p_j < g_j(M_k)-g_j(M_i)\\ \dfrac{g(M_i)+p_j-g(M_k)}{p_j-q_j}; & q_j < g_j(M_k)-g_j(M_i)\le p_j\\ 1; & g_j(M_k)-g_j(M_i)\le q_j\end{cases} \tag{2}$$

Using a similar representation, the discordance index is defined as

$$d_j(M_i,M_k)=\begin{cases}0; & g_j(M_k)-g_j(M_i) < p_j\\ \dfrac{g(M_k)-p_j-g(M_i)}{v_j-p_j}; & p_j \le g_j(M_k)-g_j(M_i)\le v_j\\ 1; & v_j < g_j(M_k)-g_j(M_i)\end{cases} \tag{3}$$

In fact, the concordance index allows the solution mechanism to determine whether M_i is at least as good as M_k with respect to the jth design criterion. In contrast, the discordance index determines whether or not a very high opposition to the outranking relation of $M_i S M_k$ (i.e., the veto condition) exists. Finally, having calculated the concordance and discordance indices with respect to all criteria, the credibility degree is obtained by

$$\delta_{ik}=C_{ik}\cdot\prod_{j\in\bar{F}}\frac{1-d_j(M_i,M_k)}{1-C_{ik}} \tag{4}$$

where $\bar{F}=\{j|j\in\{1,2,...,n\}, d_j(M_i,M_k)>C_{ik}\}$, and C_{ik} is an aggregated (global) concordance index (w_j is the weight of the jth criterion)

$$C_{ik}=\frac{\sum_{j=1}^{n} w_j c_j(M_i,M_k)}{\sum_{j=1}^{n} w_j} \tag{5}$$

The last phase of the ELECTRE III solution method is the exploitation procedure. This procedure classifies and ranks the alternatives through the so-called "descending" and "ascending" distillation processes based on the obtained credibility degrees in Eq. (4). It starts by deriving a fuzzy outranking relation between each pair of the credibility degrees. A final partial preorder Z is built by intersecting two complete preorders Z_1 and Z_2, according to the fuzzy outranking relations. The partial preorder Z_1 is defined as a partition of the criteria set into q ordered classes $\bar{B}_1,\ldots,\bar{B}_h,\ldots,\bar{B}q$, where $\bar{B}_1$ is the head-class in Z_1. Each class $\bar{B}_h$ is composed of ex-aequo elements. The complete preorder Z_2 is determined in a similar manner, where the set is partitioned into u ordered classes $\bar{B}'_1,\ldots,\bar{B}'_2\bar{B}'_h,\ldots,\bar{B}'_u$, where $\bar{B}'_u$ is the head-class. Each of these classes is defined as a final distillation. According to Z_1, the actions in class $\bar{B}_h$ are preferable to those of class $\bar{B}_{h+1}$; for this reason, distillations that lead to these classes are 'descending' (top-down). In contrast, according to Z_2, the actions in $\bar{B}_{h+1}$ are preferred to those in class $\bar{B}_h$; hence, these distillations are called 'ascending' (bottom-up). More details of the preceding procedures can be found in [28–30].

In the current case study, the ELECTRE III method resulted in the ranking/classification scheme shown in Fig. 5. The material H282 is ranked first, C263 and R-41 are nonunique (indifferent) and both ranked second, and Waspaloy is ranked last. Note that one main advantage of ELECTRE III over many other MADM methods is that it reveals indifferent alternatives; this can be

Table 8 Normalized weights (in percentage) extracted by the revised Simos' procedure (note that the sum of the weights for each designer is 100%)

	Criteria									
Designer no.	F7	F8	F9	Cr1	Cr2	M6	M4	C5	O3	D10
1	10	10	10	10	10	10	10	10	10	10
2	13.6	13.7	13.7	9.1	9.1	4.5	4.5	4.5	13.6	13.7
3	12.5	12.5	12.5	12.5	12.5	4.2	4.2	4.1	12.5	12.5
4	6.3	6.3	6.3	6.2	6.2	18.7	18.7	18.7	6.3	6.3

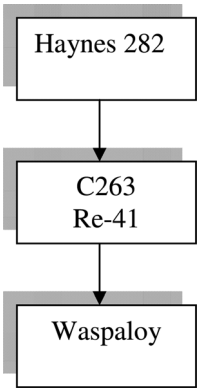

Fig. 5 Ranking and classification of the candidate superalloy materials

useful to designers not only in ranking but also identifying comparable candidate materials.

5 Conclusions

The main objective of this article was to demonstrate a framework that links the capabilities of finite element analysis (FEA) tools to the multiple attribute decision-making (MADM) approaches commonly used for structural materials selection problems. The framework was applied to the materials selection of a combustor liner where ten performance indices were identified to represent the material cost, manufacturability, oxidation resistance, damping behavior (by means of a modal strain energy method), thermomechanical properties, the fatigue, and creep behavior of four candidate superalloys for the liner wall. Subsequently, the ELECTRE III optimization method, along with the revised Simos' weighting procedure under a group decision-making environment, was employed to rank and classify the materials. The advantages of ELECTRE III include: (a) simultaneously accounting for the designers' preferences and criteria tradeoffs in the decision matrix in a noncompensatory manner, (b) allowing for uncertainties in the input data by using indifference, strict preference threshold, and veto thresholds, and (c) providing a classification of the candidate materials rather than simple ranking.

The proposed combined FEA-MADM approach may be conveniently applied to other structural materials selection problems where the ability to test preliminary designs is not economically feasible and the assessment of preliminary material systems necessitates the use of numerical prediction tools. Future work may include the introduction of an *interactive* MADM method, where interactivity is achieved by applying the method in both the early and late stages of a design. As a design process evolves, an interactive MADM model could take both the FEA results and experimental data into account and aid in establishing optimal materials and geometric parameters for complex structural designs. Finally, it should be re-emphasized that the use of ELECTRE methods for sensitive material selection applications may be motivated by the notion of 'noncompensation' between criteria. Nonetheless, other material selection methods including compensatory MADM models, reviewed by Jahan et al. [19,31], may be solved and compared to the obtained ELECTRE III solution in this case study which, in turn, can help in exploring the effect of compensation among conflicting criteria and making more comprehensive decisions.

Appendix: The Solution Steps in the Revised Simos' Method

The revised Simos' method, introduced by Figueira and Roy [27], is a tool for assigning the criteria weights in an MADM problem based on the following steps:

(a) Ranking the criteria groups from the most to the least important in an ascending order.

In this step, successive criteria (or subsets of ex-aequo criteria) are distinguished by using blank cards, if any, between them, as schematically shown in Fig. 4. Accordingly, the difference between the subset weights can be linked to the unit u used for measuring the intervals created by blank cards; n blank cards mean a difference of $n+1$ times u between two successive criteria subsets.

(b) Calculating the nonnormalized weights $P(r)$

$$P(r) = 1 + u(s_0 + \cdots + s_{r-1}) \text{ with } s_0 = 0,\ P(1) = 1 \tag{A1}$$

$$s_r = s'_r + 1\ \forall r = 1, \ldots, \bar{n} - 1 \tag{A2}$$

$$s = \sum_{r=1}^{\bar{n}-1} s_r \tag{A3}$$

$$u = \frac{z-1}{s} \tag{A4}$$

where s'_r is the number of blank cards between the rth and the $r+1$th subsets, $\bar{n}$ is the number of subsets, and z is the (importance) ratio of the most to the least important criterion defined by the decision-maker.

c) Calculating the normalized weights P^*_j

$$P' = \sum_{i=1}^{n} P'_j \tag{A5}$$

$$P^*_j = \frac{100}{P'} P'_j \tag{A6}$$

Note that within the rth subset, the criteria weights are assumed to be the same as the subset weight; i.e., if the j-criterion belongs to the rth subset $P'_j = P(r)$.

d) Minimizing the distortion of the obtained normalized weights (i.e., in case they do not sum up to 100%) using the following ratios

$$t_j = \frac{10^{-w} - \left(P^*_j - P''_j\right)}{P^*_j} \tag{A7}$$

$$\bar{t}_j = \frac{\left(P^*_j - P''_j\right)}{P^*_j} \tag{A8}$$

The P''_i is determined from P^*_i, keeping only the first wth$(w=0,1,2)$ decimal places. Here, t_i shows the dysfunction associated with the relative error rounded up to the nearest whole number, while $\bar{t}_i$ shows the dysfunction associated with the relative error rounded down to the nearest whole number.

Next, two lists, R and $\bar{R}$, are found as follows:

- The R list is made by arranging the pairs (i, t_i), ranked according to the increasing value of the ratios.
- The $\bar{R}$ list is made with the pairs $(i, \bar{t}_i)$, ranked according to the decreasing value of the ratios.

Set $L = \{i / t_i \succ \bar{t}_i\}$, $|L| = l$. The G^+ and G^- subsets with b and $N-b$ criteria, respectively, are made from G with N criteria. The criteria belonging to G^+ are rounded up to the nearest whole number, while the criteria belonging to G^- are rounded down. Finally:

- If $l + b \leq N$, then the G^- is built with the b criteria of L plus the $N - b - l$, the last criteria of $\bar{R}$ not belonging to L. The G^+ is built by the first of the b criteria of $\bar{R}$ not belonging to L; and
- If $l + b \succ N$, the list G^+ is built by the $N - b$ last criteria of R not belonging to L, plus the $b + l - N$, the first criteria of R not belonging to L. The G^- is built by the $N - b$, the last criteria of R not belonging to L.

References

[1] Shanian, A., Milani, A. S., Carson, C., and Abeyaratne, R. C., 2008, "A New Application of ELECTRE III and Revised Simos' Procedure for Group Material Selection Under Weighting Uncertainty," Knowledge Based Systems, **21**, pp. 709–720.

[2] McDanels, D. L., Serafini, T. T., and DiCarlo, J. A., 1986, "Polymer, Metal, and Ceramic Matrix Composites for Advanced Aircraft Engine Applications," J. Mater. Energy Syst., **8**, pp. 1–15.

[3] Evans, A. G., Hutchinson, J. W., and Ashby, M. F., 1999, "Multifunctional of Cellular Metal System," Prog. Mater. Sci., **43**, pp. 171–221.

[4] Rosso, M., 2006, "Ceramic and Metal Matrix Composites: Routes and Properties," J. Mater. Process. Technol., **175**, pp. 364–375.

[5] Aceves, C. M., Skordos, A. A., and Sutcliffe, M. P. F., 2008, "Design Selection Methodology for Composite Structures," Mater. Des., **29**(2), pp. 418–426.

[6] Ashby, M. F., 1992, *Materials Selection in Mechanical Design*, Pergamon, Oxford, UK.

[7] Ashby, M. F., 1993, "Criteria for Selecting the Components of Composites," Acta Metall. Mater., **41**, pp. 1313–1335.

[8] Ashby, M. F., and Bréchet, Y. J. M., 2003, "Designing Hybrid Materials," Acta Mater., **51**, pp. 5801–5821.

[9] Ashby, M. F. and Maine, E. M. A., 2000, "Design Aspects of Metal Matrix Composite Usage," *Comprehensive Composite Materials*, Vol. 3: Metal Matrix Composites, A. Kelly, C. Zweben, eds., Elseveir, Oxford, UK, pp. 779–795.

[10] Valdevit, L., Vermaak, N., Zok, F. W., and Evans, A. G., 2008, "A Materials Selection Protocol for Lightweight Actively Cooled Panels," ASME J. Appl. Mech., **75**(6), pp. 61022–61037.

[11] Sadagopan, D. and Pitchumani, R., 1998, "Application of Genetic Algorithms to Optimal Tailoring of Composite Materials," Compos. Sci. Technol., **58**, pp. 571–589.

[12] Thurston, D. L. and Carnahan, J. V., 1992, "Fuzzy Ratings and Utility Analysis in Preliminary Design Evaluation of Multiple Attributes," ASME J. Mech. Des., **114**, pp. 648–659.

[13] Karandikar, H. M., and Mistree, F., 1992, "Tailoring Composite Materials Through Optimal Selection of Their Constituents," ASME J. Mech. Des., **114**, pp. 451–459.

[14] Fitch, P. E., and Cooper, J. S., 2004, "Life Cycle Energy Analysis as a Method for Material Selection," ASME J. Mech. Des., **126**, pp. 798–805.

[15] Seepersad, C. C., Allen, J. K., McDowell, D. L., and Mistree, F., 2006, "Multifunctional Topology Design of Cellular Material Structures," ASME J. Mech. Des., **128**, pp. 499–513.

[16] Fayazbakhsh, K. and Abedian A., 2009, "Materials Selection for Applications in Space Environment Considering Outgassing Phenomenon," Adv. Space Res., **45**(6), pp. 741–749.

[17] Yoon, K. P., and Hwang, C., 1995, *Multiple Attribute Decision Making, An Introduction*, Sage, Los Angeles, CA.

[18] Milani, A. S. and Shanian, A., 2007, "Gear Material Selection With Uncertain and Incomplete Data. Material Performance Indices and Decision Aid Model," Int. J. Mech. Mater. Des., **3**, pp. 209–222.

[19] Jahan, A., Ismail, M. Y., Sapuan, S. M., and Mustapha, F., 2010, " Material Screening and Choosing Methods—A Review," Mater. Des., **31**, pp. 696–705.

[20] Pike, L. M., "Low-Cycle Fatigue Behavior of Haynes® 282®Alloy and Other Wrought Gamma-Prime Strengthened Alloys," Proceedings of ASME Turbo Expo 2007: Power for Land, Sea and Air, Montreal, Canada, May 14–17, ASME Paper No. GT2007-28267, pp. 161–169.

[21] Klinger, H., Lazik, W., and Wunderlich, T., 2008, "The Engine 3E Core Engine," Proceedings of ASME Turbo Expo 2008: Power for Land, Sea and Air, Berlin, Germany, June 9–13, ASME Paper No. GT2008-50679, pp. 93–102.

[22] Behrendt, T., Lengyel, T., Hassa, C., and Gerendas, M., 2008, "Characterization of Advanced Combustor Cooling Concepts Under Realistic Operating Conditions," Proceedings of GT2008 ASME Turbo Expo 2008: Power for Land, Sea and Air, Berlin, Germany, June 9–13, ASME Paper No. GT2008-51191, pp. 1801–1814.

[23] Johnson, C. D., and Kienhols, D. A., 1981, "Finite Element Prediction of Damping in Beams with Constrained Viscoelastic Layer," Shock Vib. Bull., **51**(1), pp. 71–81.

[24] Huang, E.-W., Barabash, R. I., Wang, Y. D., Clausens, B., Li, L., Liaw, P. K., Ice, G. E., Ren, Y., Choo, H., Pike, L. M., and Klarstrom, D. L., 2008, "Plasticity Behavior of a Nickel-Based Alloy Under Monotonic-Tension and Low-Cycle-Fatigue Loading," Int. J. Plasticity, **24**(8), pp. 1440–1456.

[25] Shanian, A., 2010, "A Modal Strain Energy Approach for Predicting of Damping of the Thermal Barrier Coating," Technical Report, Harvard University, Boston.

[26] Limarga, A. M., Duong, T. L., Gregori, G., and Clarke, D. R., 2007, "High-Temperature Vibration Damping of Thermal Barrier Coating Systems," Surf. Coat. Technol., **202**, pp. 693–697.

[27] Figueira, J., and Roy, B., 2002, "Determining the Weights of Criteria in the ELECTRE Type Methods With a Revised Simos' Procedure," Eur. J. Oper. Res., **139**, pp. 317–326.

[28] Roy, B., 1993, *Aide Multicritère à la Décision, Méthodes et Cas*, Economica, Paris, France.

[29] Figueira, J., Greco, S., and Ehrgott, M., 2005, *Multiple Criteria Decision Analysis: State of the Art Surveys*, Springer, New York.

[30] Collette, Y. and Siarry, P., 2003, *Multiobjective Optimization*, Springer, New York.

[31] Jahan, A., Ismail, M. Y., Shuib, S., Norfazidah, D., and Edwards, K. L., 2011, "An Aggregation Technique for Optimal Decision-Making in Materials Selection," Mater. Des., **32**, pp. 4918–4924.